Food Chemistry 435 (2024) 137596

Contents lists available at ScienceDirect

Food Chemistry

journal homepage: www.elsevier.com/locate/foodchem

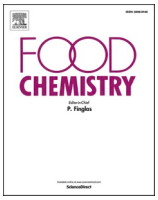

TMT quantitative proteomics analysis reveals molecular mechanism of ferroptosis during beef refrigeration

Jun Liu [a,b], Dunhua Liu [b,c,*], Ziying Hu [c,*], Yuanliang Hu [a], Xiang Yu [a]

[a] College of Life Sciences, Hubei Normal University, 435002, Huangshi, China
[b] College of Animal Science and Technology, Ningxia University, 750021, Yinchuan, China
[c] College of Food Science and Engineering, Ningxia University, 750021, Yinchuan, China

ARTICLE INFO

Keywords:
Beef
Refrigeration
Ferroptosis
Proteomics
Meat quality

ABSTRACT

Ferroptosis is a recently identified cell death process in refrigerated beef, and its mediated protein oxidation and cell death may reduce muscle quality, but the mechanism of ferroptosis is unclear. In the study, free iron accumulation reached 19.670 ± 0.482 μg/g after 6 days refrigeration, the levels of apoptosis, ROS, and lipid peroxidation increased significantly ($P < 0.05$), and muscle tissue cells exhibited typical ferroptosis characteristics. A total of 377 differentially expressed proteins (DEPs) were identified by TMT quantitative proteomics. 15 DEPs, including transferrin, ferritin, glutathione peroxidase (GPX) 4, and heme oxygenase 1, were involved in lipid peroxidation, Fe^{2+} and Fe^{3+} conversion, iron ion accumulation, and mitochondrial oxidative stress to induce ferroptosis. In addition, signalling pathways, such as chemical carcinogenesis-ROS, glutathione metabolism, HIF-1, and PPAR may promote ferroptosis by affecting free iron overload and GPX4 inactivation.

1. Introduction

Beef is among the most widely consumed meats worldwide (Liu, Ellies-Oury, Stoyanchev & Hocquette, 2022). Beef quality is of critical importance to consumers, who evaluate the quality of beef based on appearance, including colour and juice loss. Consumers' evaluation of beef quality determines purchase decision, which is critical to the beef market and the growth of the industry (Liu et al., 2022; Pogorzelski, Pogorzelska-Nowicka, Pogorzelski, Półtorak, Hocquette & Wierzbicka, 2022). The discovery of the elements and mechanisms involved in influencing beef quality is relevant to improving meat quality and increasing the commercial value of meat. The ageing process of post-slaughter muscle is critical to the meat quality. After slaughter, muscle tissue cells begin to undergo many forms of death, such as necrosis, apoptosis, pyroptosis, and autophagy, which is the first step in the transformation of muscle into meat. This process triggers a complex chain of biochemical reactions, including the escape of intracellular components and cell contraction, which structurally change muscle fibrous proteins (Zhang et al., 2013). The quality of meat, including colour, water-holding capacity, tenderness and flavour, has been linked to cell death in recent studies (Gagaoua, Terlouw & Picard, 2017; Guo et al., 2016; Tian, Li, Shi & Chen, 2022). Ferroptosis is the most recently identified form of cell death during beef ageing (Liu, Hu, Liu, Zheng & Ma, 2023; Liu, Hu, Ma, Wang & Liu, 2023). However, to our knowledge, the mechanisms by which ferroptosis occurs are unclear.

Ferroptosis is an iron-dependent death characterised by the excessive accumulation of lipid peroxides in the plasma membrane due to iron overload, ultimately leading to oxidative damage to the cell membrane and cell death (Yang & Stockwell, 2016). Iron is the hub of ferroptosis, with excess free Fe^{2+} accumulating in the cytoplasm and Fe^{2+} generating large amounts of hydroxyl radicals and reactive oxygen species (ROS) via the Fenton reaction. Intracellular iron overload is complex and diverse, transferrin receptor protein (TFR) 1 on the surface of the cell membrane recognises transferrin (TF), which is then transferred to the cytoplasm via SLC11A2 (Ma, Chen, Zhu, Zhang, Zhou & Duan, 2022). In addition, the degradation of iron-containing proteins, such as ferritin and heme, also causes the accumulation of free iron in the cell. Another feature of ferroptosis is the disruption of the intracellular redox system. The System Xc^- glutathione (GSH) - glutathione peroxidase (GPX) 4 system, the main preventive pathway for ferroptosis, results in the loss of function of the ferroptosis reduction system due to a decrease in GSH synthesis (Forcina & Dixon, 2019; Gaschler & Stockwell, 2017). Also, other antioxidant systems are involved in the regulation of ferroptosis, including the *trans*-sulfuration pathway and the mevalonate

* Corresponding authors at: No.489, Mount Helan West Road, Xixia District, Yinchuan City, 750000, Ningxia, China.
E-mail addresses: ldh320@nxu.edu.cn, dunhualiu@126.com (D. Liu), 13350653505@163.com (Z. Hu).

https://doi.org/10.1016/j.foodchem.2023.137596
Received 11 May 2023; Received in revised form 15 September 2023; Accepted 23 September 2023
Available online 26 September 2023

pathway (Ma, Chen, Zhu, Zhang, Zhou & Duan, 2022). In brief, the proteins and metabolites involved in these pathways are complex and diverse. We have previously determined the ferroptosis process during beef ageing through a metabolomic approach (Liu et al., 2023). Nevertheless, revealing the mechanism of ferroptosis in beef from protein or enzyme perspectives has rarely been reported.

The protein alteration processes responsible for differences in meat quality have been studied by a variety of technologies. Dynamic changes identification in protein composition and content in animal, plant and microbial samples from different sources, substances or growth stages are possible with proteomics investigations, which also provide global detection and quantification of proteins (Luan et al., 2022). It is now widely utilized in the inspection and analysis of food products, and this work has helped elucidate the mechanisms underlying meat ageing and quality. Proteomics approaches have been used to assess potential mechanisms of change in meat quality, such as flavor, color and tenderness (Jia, Shi, Zhang, Shi & Chu, 2021; Jia, Zhang, Liu, Zhu, Xu & Shi, 2021; Joseph, Nair & Suman, 2015). In addition, Liu, Liu, Wu, Pan, Wang & Ma. (2022) investigated the molecular mechanisms of transport stress on liver iron metabolism in chickens through proteomics. These studies show that proteomic strategies are feasible for studying the molecular change patterns during beef storage, the mechanisms of ferroptosis in beef, or identifying the proteins involved in ferroptosis and the discovery of protein biomarkers.

In the study, the beef quality and physiological and biochemical changes during cold storage were evaluated, and a tandem mass tags (TMT)-liquid chromatography (LC)-high-resolution tandem mass spectrometry (MS) proteomics strategy was used to determine the expression levels of the proteins and pathways involved in ferroptosis in beef during refrigeration. To validate the screened proteins, targeted method-parallel reaction monitoring (PRM) was used to analyse the expression of relevant proteins. Our results provide valuable clues to the physiological and molecular mechanisms of ferroptosis during post-slaughter beef storage, as well as novel strategies for improving beef quality.

2. Materials and methods

2.1. Sampling and treatment

Eight adult Qinchuan cattle (bulls, 18–24 months of age, weighing approximately 400 kg) were slaughtered at a commercial slaughterhouse (Yitai Co., Yongning, China) according to Chinese livestock slaughter protocols. Muscle samples (*M. longissimus lumborum* muscles) were collected after slaughter. The muscle sample segmentation and storage conditions were described in our previous reports (Liu et al., 2023; Liu, Liu, Zheng & Ma, 2022). Briefly, *M. longissimus lumborum* muscles samples were collected after slaughter, and the muscle samples were divided into cubes with sides of 2.5 cm thickness and 100.0 ± 2.5 g weight, placed onto PET plastic trays and wrapped in polyvinyl chloride cling film. The samples were divided into 5 groups (8 muscle samples each group) and stored in an open refrigerated display cabinet for 6 days to simulate a beef marketing scenario. Divided finished muscle was defined as 0 days (B0), and 24 h, 48 h, 96 h, and 144 h refrigerated finished muscle was defined as 1, 2, 4, and 6 days (B1, B2, B4, and B6). Samples were collected from muscle tissue centers at 0, 1, 2, 4, and 6 days, fresh samples were used to test meat quality and stored at −80 °C after quick freezing in liquid nitrogen for further analyses.

2.2. Evaluation of beef quality

The hardness (gf) was determined by a texture tester (TAXTC10014, Shanghai Baosheng Industrial Development Co., Ltd., Shanghai, China) with the following parameters: pre-test probe descent speed: 60 mm/min; post-test probe rise speed: 60 mm/min; test speed: 60 mm/min; distance: 30 % strain; trigger type: 20 mm sample rise height. To determine the drip loss rate, in brief, muscle weighing approximately 10 g was hung on plastic hooks in the shape of an “S” in a refrigerator at 4 °C, covered with a plastic bag and tied tightly, and then taken out and weighed 24 h later. The drip loss rate was expressed as a percentage of mass loss before and after hanging. Changes in the color of beef during refrigeration were measured by a CR-410 handheld colorimeter (Minolta Co., Ltd., Osaka, Japan), and the results were expressed as L* (lightness), a* (redness) and b* (yellowness), with a total of five measurements for each sample (Liu, Hu, Zheng, Ma & Liu, 2022; Liu, Liu, Wu, Pan, Wang & Ma, 2022).

2.3. Muscle tissue ROS levels

ROS levels in muscle tissue were measured by the 2,7-dichlorofluorescein diacetate (DCFH-DA) method according to Zhang, Yu, Han, Han & Han. (2020). Briefly, 5.00 ± 0.05 g of pulverized muscle samples were mixed with 20 mL of prechilled potassium phosphate buffer (10 mM Tris, 10 mM sucrose, 0.8 % NaCl, 0.1 mM EDTA-2Na, pH 7.4), and then homogenized for 60 s and centrifuged at 10,000 × g, 4 °C for 20 min. Then, 5 mL supernatant were mixed with 5 mL potassium phosphate buffer (containing 10 μM DCFH-DA) and incubated at 37 °C in the dark for 35 min. A fluorescence spectrophotometer (Yidian Scientific Instruments Co., Shanghai, China) with an excitation wavelength of 480 nm and an emission wavelength of 525 nm was used to measure the fluorescence intensity before and after incubation. The ROS level was expressed as the ratio of fluorescence intensity before and after incubation to protein concentration and incubation time.

2.4. TUNEL staining for apoptosis

The TUNEL kit (Jiancheng Institute of Biological Engineering, Nanjing, China) was used to stain the nuclei of apoptotic cells in muscle tissue (Liu et al., 2023). Samples were taken from the center of the muscle, divided into 0.5 × 0.5 × 0.5 cm blocks using a medical scalpel and placed in 20 × volume of 4 % paraformaldehyde solution for 24 h. After paraffin embedding, paraffin sections (10 μm) of muscle tissue were prepared using a rotary pathology microtome (Taiwei Co Ltd., Hubei, China). The sections were processed according to the kit instructions, and images were captured by Eclipse C1 fluorescence microscope (Nikon, Tokyo, Japan). The nuclei of muscle tissue sections showed blue fluorescence, and the nuclei of apoptotic cells showed green fluorescence in the images. Four different positions were randomly selected for each image (50 μm), and the number of nuclei and positive nuclei was counted (10 μm). The rate of apoptosis in muscle tissue is expressed as the percentage of positive nuclei (apoptotic cells) to the total nuclei after staining.

2.5. Determination of free iron content

Briefly, 30 g of muscle were minced, and 10.00 ± 0.02 g of minced meat were added into 100 mL of deionized water, then homogenized for 60 s and centrifuged at 12,000 × g for 10 min. The supernatant was separated through an Amicon Ultra-15 ultrafiltration centrifuge filter (3,000 MW cut-off), centrifuged at 4,500 × g for 50 min, and the liquid was collected at the bottom of the centrifuge tube. Then 4 mL of the filtrate was pipetted and the free iron content was measured by ICP-OES (Agilent, Santa Clara, CA, USA) (Liu et al., 2023).

2.6. Ferroptosis characteristic indicator testing

The levels of malondialdehyde (MDA), glutathione (GSH), and GPX4 in muscle tissue were measured using an assay kit (Jiancheng Co., Nanjing, China). Muscle tissues were added to 9 times the volume of precooled 0.9 % NaCl solution, ground and homogenized, and centrifuged at 14,000 × g, 4 °C for 10 min. The supernatant was collected and the levels of MDA, GSH, and GPX4 analyzed using a UV spectrophotometer by measuring the absorbance values at 532 nm, 420 nm and 450 nm

respectively (Liu, Hu, Zheng, Ma & Liu, 2022).

2.7. TMT quantitative proteomics analysis

2.7.1. Muscle protein extraction

Each muscle sample was added to 800 μL SDT extraction buffer (50 mM Tris-HCl, 4 % SDS, 100 mM NaCl, pH 8.0), crushed, grinded and homogenised for 2 min. Then the mixture was sonicated in an ice-water bath for 2 min and centrifuged at 16,000 × g, 4 °C for 20 min. The supernatant was then collected to obtain the protein solution.

2.7.2. TMT peptide labeling and LC-MS/MS analysis

Protein digestion, TMT peptide labelling, peptide classification, and LC-MS/MS analysis were performed referring to our previous method (Liu et al., 2022). In brief, protein extracts from muscle samples were subjected to enzymatic digestion, and purified peptides were collected. The extracted peptides were labelled using TMT labelling kits according to the manufacturer's instructions. The dried peptides were fractionated, separated, and analyzed using a Pierce™ high pH reversed-phase peptide fractionation kit, nanolitre flow rate chromatography system and data dependent acquisition (DDA) mass spectrometry (Thermo Fisher, MA, USA).

2.7.3. Database search

The resulting LC-MS/MS raw RAW files were imported into the search engine Sequest HT in Proteome Discoverer software (version 2.4, Thermo Scientific, San Jose, USA) for database searching. The database used for the library search was uniprot-Bos taurus (Bovine) [9913]-47135–20220613.fasta from the URL https://www.uniprot.org/taxonomy/9913 protein database with protein entry: 47135; download date: 2022.06.13.

2.7.4. Bioinformatics analysis

The data were analysed using Perseus software, Microsoft Excel, and R statistical computing software. Protein expression data were grouped according to protein level by hierarchical clustering. The information was extracted from UniProtKB/Swiss-Prot, the Kyoto Encyclopedia of Genes and Genomes (KEGG) and Gene Ontology (GO) were used to annotate sequences. Enrichment analyses were performed using Fisher's exact test with FDR correction for multiple trials.

2.8. Liquid chromatography-parallel reaction monitoring/mass spectrometry (LC-PRM/MS)

Based on the previous TMT proteomics results (**Table S1**), proteins related to the ferroptosis pathway were selected as target peptides for LC-PRM/MS target property profiling for quantitative PRM analysis. The peptide information screened for PRM analysis was entered into the Xcalibur 4.0 Software (Thermo Scientific, San Jose, USA) referring to the TMT proteomics peptide processing and chromatography system, and 2 μg of each sample was taken for PRM analysis. The peptides were separated and then analysed by targeted PRM mass spectrometry using a QExactive HF-X mass spectrometer (Thermo Scientific, San Jose, USA). The detection time of the mass spectrometry scan was 60 min. The detection modes were positive and parent ions. The scan range was 300–1200 *m/z*, primary mass resolution was 60,000 @*m/z* 200, AGC target was 3e6, and primary mass Maximum IT was 50 ms. After the full MS scan, the target peptides were selected in order of their Precursor *m/z* by referring to the Inclusion list. After the full MS scan was completed, the MS2 scan was performed with a resolution of 30,000 @ *m/z* 200, AGC target: 1e6, Maximum IT: 100 ms, MS2Activation Type: HCD, Isolation window: 1.6 Th, Normalized collision energy: 28. The raw RAW files of the obtained mass spectra were analysed for PRM data using the software Skyline 4.1.

2.9. Statistical analysis

All physical and chemical indicators were tested three times and expressed as mean ± standard deviation. One-way analysis of variance (ANOVA) was performed using SPSS, and $P < 0.05$ was considered to be a significant difference. Figures were plotted using R project (R version 4.0.5). Fig. 3 was drawn using the Figdraw online drawing program from HOME for Researchers (License ID: ID:RRUTU50ff4).

3. Results

3.1. Characteristics of beef quality

Hardness was used to characterize the tenderness of beef, with prolonged refrigeration hardness decreased significantly ($P < 0.05$) at 4 and 6 days, with hardness values decreasing by 39.75 % (Table 1). Drip loss indicates the water holding capacity of beef, and the drip loss rate showed a significant ($P < 0.05$) increase throughout the whole period of refrigeration, indicating that the ability of beef to hold water decreases with prolonged refrigeration. L*, a*, and b* were used to characterize the change of beef colour. The trend of change of the L* and b* values was consistent, which was significantly decreased at 4d and 6d, and the a* value showed a significant ($P < 0.05$) decrease throughout the whole period of refrigeration. The L* value reflects the brightness of the meat, b* represents yellowish blue and a* represents reddish green. The overall decreasing trend of L*, a*, and b* value indicates that the beef colour darkens and loses its luster, and the bright red colour changes to dark red.

3.2. Characteristics of ferroptosis in muscle tissue

Free iron, ROS, lipid peroxides, MDA, GSH, and GPX4 levels were measured to assess the ferroptosis status of muscle tissue cells. As shown in Table 1, the levels of free iron, ROS, and MDA increased significantly with refrigeration time (by 387.2 %, 176.4 %, and 73.3 %, respectively). In contrast, GSH and GPX4 levels were significantly lower at 6 d than at

Table 1
Characteristics of ferroptosis in muscle tissue during refrigeration.

Refrigeration time (days)	0d	1d	2d	4d	6d
Hardness (gf)	1852.44 ± 134.69^{a}	1725.29 ± 113.19^{a}	1713.09 ± 111.35^{a}	1230.82 ± 81.36^{b}	1116.10 ± 138.02^{b}
Drip loss (%)	0.160 ± 0.013^{e}	0.208 ± 0.007^{d}	0.275 ± 0.016^{c}	0.35 ± 0.018^{b}	0.432 ± 0.027^{a}
L*	33.17 ± 0.90^{b}	35.67 ± 1.06^{a}	32.18 ± 1.22^{bc}	30.88 ± 1.09 ^{cd}	29.27 ± 1.30^{d}
a*	21.45 ± 0.91^{a}	19.78 ± 1.57^{a}	15.22 ± 1.24^{b}	10.75 ± 1.36^{c}	13.27 ± 0.94^{d}
b*	5.47 ± 1.02^{b}	6.75 ± 1.35^{a}	5.08 ± 1.36^{bc}	3.45 ± 1.28^{c}	2.15 ± 1.26 ^{cd}
Free iron content (μg/g)	4.037 ± 0.050^{e}	9.237 ± 0.069^{d}	11.547 ± 0.102^{c}	13.633 ± 0.078^{b}	19.670 ± 0.482^{a}
Apoptosis rate (%)	0.134 ± 0.070^{e}	0.479 ± 0.080^{d}	1.005 ± 0.100^{c}	2.450 ± 0.094^{b}	3.743 ± 0.099^{a}
ROS level (Fluorescence intensity/mg/L/min)	88.900 ± 3.400^{e}	107.300 ± 4.700^{d}	185.400 ± 2.900^{c}	207.900 ± 6.900^{b}	245.700 ± 5.500^{a}
MDA content (μmol/mg prot)	1.011 ± 0.086^{d}	1.360 ± 0.039^{c}	1.445 ± 0.005^{b}	1.448 ± 0.002^{b}	1.752 ± 0.011^{a}
GSH content (U/mg prot)	12.269 ± 0.882^{a}	10.811 ± 0.231^{b}	9.127 ± 0.162^{c}	7.512 ± 0.737^{d}	4.734 ± 0.374^{e}
GPX4 content (ng/mL)	11.041 ± 0.959^{a}	10.507 ± 1.072^{a}	8.628 ± 0.593^{b}	5.777 ± 1.219^{c}	4.572 ± 0.709^{c}

Note: Different letters (a-e) in the same row indicate a significant difference ($P < 0.05$).

0 d ($P < 0.05$). Apoptosis rates significantly increased during refrigeration ($P < 0.05$).

3.3. Proteomic profile

Muscle samples from different refrigeration periods were used to extract proteins and then subjected to SDS-PAGE analysis. The protein bands were evenly distributed and similar among different periods in the 1D mode (Fig. 1**a**). The expression distribution of the sample proteins was analyzed based on the expression status of the proteins among different samples. The sample expression distribution plot showed that the median of the samples in the same group was close to the same level (Fig. 1**b**), indicating that the muscle sample proteins had good intra-group similarity and inter-group variability.

3.4. Differentially expressed proteins (DEPs)

The mass spectrometry results were imported into the database, and a total of 1996 proteins were identified. Proteins identified from B1, B2, B4, and B6 were screened for differential expression using B0 as the control group. The volcano plot was visualized and analyzed for DEPs based on two criteria: FC > 1.2, FC < 0.86 and $P < 0.05$. As shown in Fig. 1 c-f, 22, 33, 73, and 140 DEPs were identified in B1/B0, B2/B0, B4/B0, and B6/B0, of which 6, 11, 32, and 88 were up-regulated and 16, 22, 41, and 52 down-regulated. Muscle protein expression differences were increased as storage time increased. A total of 377 DEPs were identified (Fig. 1**g**), and the expression of proteins in muscle tissues at different refrigeration stages was evaluated using clustering. The clustering heat map was colored differently, with red indicating the up-regulation of protein expression and blue indicating the down-regulation of protein expression.

3.5. Functional analysis of DEPs

As shown in Fig. 2**a**, the main functions of these DEPs include biological process (BP), molecular function (MF), and cellular component (CC). The GO functional analysis showed that DEPs in the BP group were mainly involved in cellular processes (148), metabolic processes (116), biological regulation (78), regulation of biological processes (74), and response to stimulus (57). The DEPs in the MF group were mainly involved in binding (114), catalytic activity (75), etc. DEPs in the CC group were mainly involved in cellular anatomical entities (171) and protein-containing complexes (56), etc.

3.6. Ferroptosis pathways involved in DEPs

To clarify the functions and pathways of DEPs involved in cells and organisms at the molecular level, DEPs were enriched into KEGG pathways for annotation and identification. The top 20 enriched pathways are shown in Fig. 2**b**, including ferroptosis, Huntington's disease, amyotrophic lateral sclerosis, pathways of neurodegeneration-multiple diseases, carbon metabolism, the citric acid cycle (TCA cycle), and oxidative phosphorylation. As shown in Table 2, a total of 15 DEPs involved in the ferroptosis pathway were identified. Ferric ion transport proteins include voltage-dependent anion-selective channel protein 2, voltage-dependent anion-selective channel protein 3, serotransferrin, and transferrin receptor protein 1. Divalent and trivalent ferric ion conversion proteins include ceruloplasmin, major prion protein, poly (rc)-binding protein 1, and poly (RC) binding protein 2. Ferroptosis regulatory proteins include arachidonate-coa ligase, acyl-coa synthetase long chain family member 4, lysophospholipid acyltransferase 5, and acyl-coa synthetase long chain family member 3.

3.7. Pathways and protein interactions associated with ferroptosis

To further explore the pathway-pathway interactions associated with ferroptosis, KEGG-enriched pathway analysis was performed with the identified 15 DEPs. The top 20 relevant pathways involved in the ferroptosis (Fig. 2**c**) mainly included cellular processes, environmental information processing, metabolism, and organismal system. Ferroptosis was an essential process of cellular senescence and necroptosis. Notably, 38 differentially expressed proteomes were involved in a total of 38 pathways (Fig. 2**d**). Protein interaction analysis showed that, except for VDAC3 and PRNP, all the proteins interacted with each other to regulate ferroptosis (Fig. 2**e**). Subcellular localization analysis of the identified DEPs involved in ferroptosis revealed that the metabolic processes involved in ferroptosis occurred mainly in the cytoplasm, endoplasmic reticulum, mitochondrion, membrane, golgi apparatus and extracellular region (Fig. 2 f and g).

3.8. PRM validation of DEPs involved in the ferroptosis pathway

Based on the results of TMT quantitative proteomic analysis, 15 proteins involved in the regulation of ferroptosis were selected for PRM quantification validation. As shown in **Table S1**, each protein contained at least 1 unique peptide, which was validated by PRM with quantitative data of the target peptide fragments due to the requirement of protein identity and abundance. The ion abundance of the 15 proteins involved in the ferroptosis pathway followed the same trend as the TMT quantitative protein assay, with 8 up-regulated and 7 down-regulated DEPs (Table 3).

4. Discussion

Ferroptosis, as one of the forms of cell death, affects muscle quality through various physiological and biochemical metabolisms (Liu et al., 2022). Notably, the degree of ferroptosis was characterized by the characteristic physiological changes during ferroptosis (Table 1) where free iron accumulation, oxidative stress and increased apoptosis rates exhibited typical ferroptosis characteristics. Oxidative stress and cell death are considered important factors affecting muscle quality. ROS generated in the ferroptosis pathway attack lipids and proteins in muscle tissue, inducing polyunsaturated fatty acid damage and leading to the formation of α- and β-unsaturated aldehydes, as well as protein fragmentation, amino acid cross-linking, and peptide side-chain modification, which have the direct effect of affecting the structure of muscle fibers (Guo et al., 2016). The cell death process, on the other hand, destroys the integrity of the tissue cells and also causes the release of intracellular substances, such as water, proteases and metal ions (Zhang et al., 2013). Both affect muscle quality by altering the structure of muscle tissue. The structural integrity of muscle fibers determines the hardness of muscle tissue, and protein fragmentation or degradation leads to the loss of structural integrity of muscle fibers, which is directly reflected in the reduction of hardness. Cellular integrity facilitates water immobilization, and cellular damage accelerates water escape. Changes in muscle color are closely related to the oxidation of heme (Gagaoua, Terlouw & Picard, 2017; Joseph, Nair & Suman, 2015). Muscle tissue underwent significant changes in stiffness, water holding capacity, and color (Table 1**)**. However, the conversion of normal aerobic metabolism of cells to anaerobic metabolism after slaughter, oxidative stress and other metabolic activities also lead to cell death, exhibiting partial ferroptosis characteristics (Lana et al. (2015)). Notably, the ferroptosis was a complex and interconnected process, with protein–protein interactions, and pathway-pathway interactions being involved (Fig. 2 d and e). All of these processes can be potential killers of muscle quality. Therefore, the expression patterns of proteins involved in the regulation of ferroptosis need to be further explored to elucidate the mechanism of ferroptosis in muscle tissue.

4.1. Cell membrane iron ion transport pathway

The ferroptosis process was largely dependent on intracellular iron

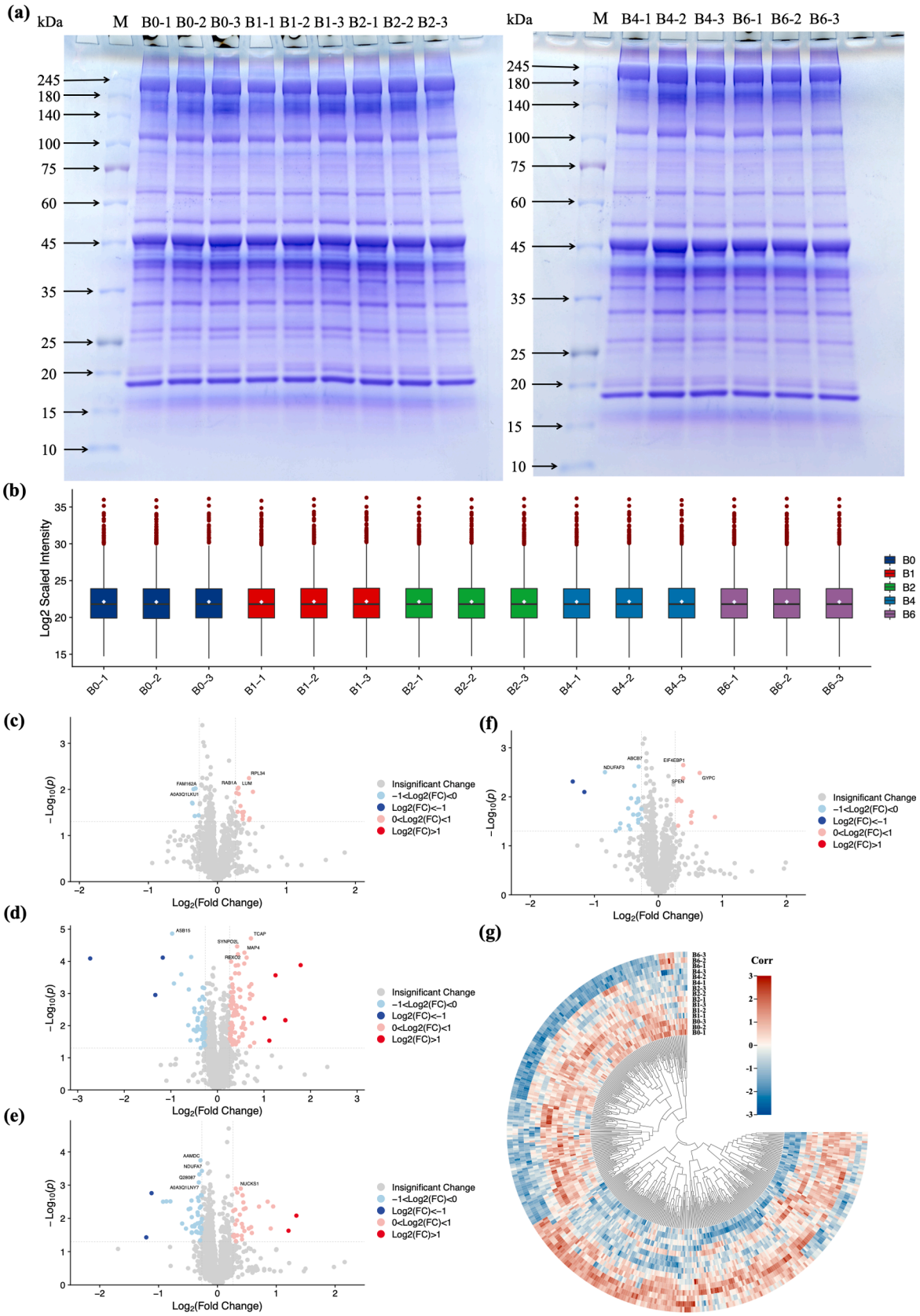

Fig. 1. (a) Protein profile determined by SDS-PAGE gel electrophoresis. (b) Box plot of sample protein expression distribution. (c) Volcano plots of DEPs between Group B0 and B1. (d) Volcano plots of DEPs between Group B0 and B2. (e) Volcano plots of DEPs between Group B0 and B4. (f) Volcano plots of DEPs between Group B0 and B6. (g) Heat map of clustering of DEPs.

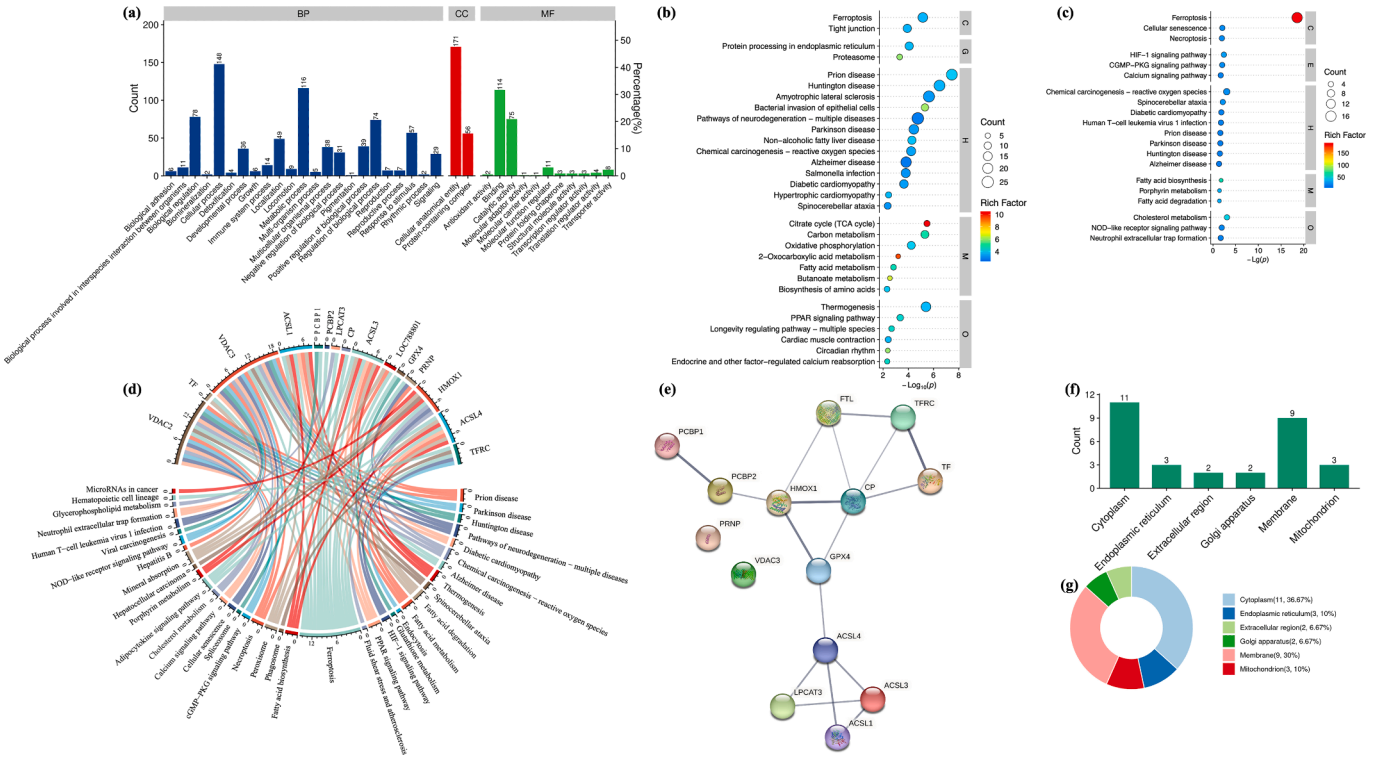

Fig. 2. (a) GO functional annotation of DEPs. BP indicates biological process, CC indicates cellular component, and MF indicates molecular function. (b) Enrichment analysis of the DEPs KEGG pathway. (c) KEGG pathway analysis using 15 DEPs obtained by screening ferroptosis. C indicates cellular process, E indicates environmental information processing, G indicates genetic information processing, H indicates disease, M indicates metabolism, and O indicates organismal system. (d) String diagram of the interaction between DEPs involved in the regulation of ferroptosis and related pathways. (e) Interaction network diagram of DEPs involved in the regulation of ferroptosis. (f-g) Subcellular localization of the 15 DEPs obtained from the ferroptosis pathway based on GO functional annotation.

Table 2
Differentially expressed proteins involved in ferroptosis based on KEGG enrichment pathway screening.

Num.	Uniport ID	Protein name	Gene name	Log_{10} B0	Log_{10} B1	Log_{10} B2	Log_{10} B4	Log_{10} B6
1	P68002	Voltage-dependent anion-selective channel protein 2	TF	8.165 ± 0.006	8.179 ± 0.025	8.180 ± 0.006	8.191 ± 0.010	8.215 ± 0.010
2	G3X6N3	Serotransferrin	TF	7.845 ± 0.005	7.856 ± 0.050	7.908 ± 0.023	7.910 ± 0.020	7.912 ± 0.047
3	Q9MZ13	Voltage-dependent anion-selective channel protein 3	VDAC3	7.991 ± 0.031	7.959 ± 0.010	7.955 ± 0.036	7.954 ± 0.004	7.936 ± 0.014
4	A0A3Q1M3G1	Arachidonate-CoA ligase	ACSL1	8.025 ± 0.016	8.050 ± 0.022	8.047 ± 0.010	8.054 ± 0.010	8.068 ± 0.021
5	Q5E9A3	Poly(rC)-binding protein 1	PCBP1	7.485 ± 0.008	7.482 ± 0.003	7.471 ± 0.031	7.457 ± 0.014	7.446 ± 0.004
6	Q3SYT9	Poly(RC) binding protein 2	PCBP2	5.697 ± 0.037	5.676 ± 0.029	5.669 ± 0.036	5.666 ± 0.013	5.651 ± 0.018
7	G8JL05	Lysophospholipid acyltransferase 5	LPCAT3	7.055 ± 0.010	7.056 ± 0.012	7.058 ± 0.006	7.061 ± 0.021	7.077 ± 0.018
8	A0A3Q1MI22	Ceruloplasmin	CP	6.123 ± 0.015	6.119 ± 0.031	6.091 ± 0.044	6.090 ± 0.005	6.046 ± 0.056
9	F1MEX9	Acyl-CoA synthetase long chain family member 3	ACSL3	5.715 ± 0.014	5.729 ± 0.004	5.734 ± 0.015	5.736 ± 0.028	5.753 ± 0.043
10	A0A3Q1MF87	Ferritin	LOC788801	5.296 ± 0.022	5.275 ± 0.023	5.274 ± 0.029	5.251 ± 0.041	5.236 ± 0.017
11	Q9N2J2	Phospholipid hydroperoxide glutathione peroxidase	GPX4	6.097 ± 0.022	6.096 ± 0.031	6.076 ± 0.006	6.064 ± 0.031	6.059 ± 0.064
12	D5G2D5	Major prion protein	PRNP	6.509 ± 0.013	6.501 ± 0.013	6.496 ± 0.022	6.474 ± 0.010	6.445 ± 0.014
13	Q5E9F2	Heme oxygenase 1	HMOX1	6.008 ± 0.015	6.059 ± 0.016	6.007 ± 0.047	6.098 ± 0.045	6.134 ± 0.038
14	A0A3Q1LZ55	Acyl-CoA synthetase long chain family member 4	ACSL4	5.340 ± 0.024	5.355 ± 0.027	5.354 ± 0.024	5.412 ± 0.012	5.416 ± 0.016
15	E1BIG6	Transferrin receptor protein 1	TFRC	5.609 ± 0.012	5.613 ± 0.020	5.622 ± 0.045	5.632 ± 0.036	5.642 ± 0.059

Table 3
Quantitative analysis of PRM for ferroptosis protein peptides.

Gene name	Unioort ID	Relative abundance of PRM normalized ion peak area				
		B0	B1	B2	B4	B6
TF	P68002	1.00 ± 0.00	1.035 ± 0.058	1.037 ± 0.014	1.062 ± 0.023	1.122 ± 0.026
TF	G3X6N3	1.00 ± 0.00	1.030 ± 0.120	1.156 ± 0.059	1.162 ± 0.053	1.173 ± 0.126
VDAC3	Q9MZ13	1.000 ± 0.00	0.926 ± 0.021	0.921 ± 0.075	0.916 ± 0.009	0.878 ± 0.028
ACSL1	A0A3Q1M3G1	1.000 ± 0.00	1.060 ± 0.055	1.054 ± 0.025	1.069 ± 0.024	1.107 ± 0.053
PCBP1	Q5E9A3	1.000 ± 0.00	0.994 ± 0.008	0.971 ± 0.067	0.938 ± 0.032	0.914 ± 0.009
PCBP2	Q3SYT9	1.000 ± 0.00	0.946 ± 0.072	0.930 ± 0.085	0.920 ± 0.031	0.885 ± 0.040
LPCAT3	G8JL05	1.000 ± 0.00	1.001 ± 0.028	1.007 ± 0.015	1.015 ± 0.050	1.053 ± 0.049
CP	A0A3Q1MI22	1.000 ± 0.00	0.994 ± 0.076	0931 ± 0.099	0.924 ± 0.012	0.839 ± 0.116
ACSL3	F1MEX9	1.000 ± 0.00	1.035 ± 0.010	1.048 ± 0.041	1.057 ± 0.074	1.106 ± 0.123
LOC788801	A0A3Q1MF87	1.000 ± 0.00	0.938 ± 0.067	0.938 ± 0.085	0.875 ± 0.115	0.829 ± 0.045
GPX4	Q9N2J2	1.000 ± 0.00	0.999 ± 0.073	0.951 ± 0.015	0.927 ± 0.067	0.923 ± 0.142
PRNP	D5G2D5	1.000 ± 0.00	0.981 ± 0.030	0.970 ± 0.048	0.920 ± 0.022	0.860 ± 0.028
HMOX1	Q5E9F2	1.000 ± 0.00	1.130 ± 0.044	1.187 ± 0.133	1.248 ± 0.138	1.356 ± 0.125
ACSL4	A0A3Q1LZ55	1.000 ± 0.00	1.047 ± 0.084	1.044 ± 0.074	1.230 ± 0.043	1.243 ± 0.056
TFRC	E1BIG6	1.000 ± 0.00	1.012 ± 0.055	1.041 ± 0.121	1.065 ± 0.102	1.102 ± 0.171

overload (Fig. 3 **and S1**). Most of the extracellular iron exists as free iron (Fe^{3+}), and the transmembrane transport of Fe^{3+} first requires binding to circulating transferrin, thus triggering endocytosis of the transferrin bound iron (TBI)-transferrin receptor (TFR) 1 complex and transfer into the cell via the Fe^{3+}-TFR1 pathway (Stoyanovsky et al., 2019). In the acidic environment of the endosome, iron is released from the transferrin complex and converted from Fe^{3+} to Fe^{2+} by the STEAP family of iron reductases. Subsequently, endosome (a membrane-encapsulated vesicular structure) iron can be transported across the membrane to the cytoplasm via the membrane transporter divalent metal transporter (DMT) 1 or the multispecific metal transporter ZRT/IRT-like protein (ZIP 14/8) (Ma et al., 2022). It was reported that the transport of Fe^{3+} by prion protein (PRNP) on the cell membrane was not dependent on the TBI-TFR1 transport system and that PRNP can convert Fe^{3+} to Fe^{2+} by transferring it into the cell via the zinc transporter on the cell membrane (ZIP8/ZIP14) (Xiong et al. (2022)). PRNP was not correlated with TF and TFR1 (Fig. 2**e**), further validating the unique iron ion transport mechanism of PRNP. Nevertheless, some cells do not bind to transferrin during iron transport and are transported directly into the cytoplasm via cell surface transporters without endocytosis (Zhao, Gao, Enns & Knutson, 2010). This iron transport process was found only in intestinal epithelial cells (Zhao et al., 2010), therefore, we hypothesize that the iron transport process in muscle tissue cells may proceed predominantly through TFR1. Stoyanovsky et al., (2019) reported that when cells were in a pathological or stressful state, non-transferrin-bound iron was not dependent on endocytosis and can be transported directly into the cell via transporters. After the muscle tissue was divided, the non-normal physiological state of iron transport may be activated, which may be one of the pathways of intracellular iron overload. As shown in Table 2 and Fig. 3, the iron transport proteins are upregulated during muscle refrigeration, and the upregulation of the iron transport proteins and receptor proteins indicates an enhancement of the iron transport process, which induces intracellular iron overload.

4.2. Ferritin and heme degradation pathways

Degradation of iron-containing protein complexes is also one of the important pathways that cause intracellular iron accumulation. The production of ROS from free iron via the Fenton reaction is a central aspect of ferroptosis and has a direct influence on the muscle (Liu et al., 2023). Iron stored in intracellular ferritin can be released into the cytoplasm via the lysosomal-ferritin autophagic pathway (Liu et al., 2023). Nuclear receptor coactivator (NCOA) 4 can regulate the transcription of nuclear genes or bind to ferritin to activate the ferritin autophagy pathway and direct ferritin into the autophagosome for degradation and release of ferric ions (Mancias, Wang, Gygi, Harper & Kimmelman, 2014). Iron ions released from ferritin within the lysosome can be transported outside the cell through the cell membrane or into the mitochondria where they are converted into mitochondrial iron cofactors (hemoglobin, Fe-S clusters, non-hemoglobin iron centers) (Dowdle et al., 2014). These iron ions undergo reduction by the intracellular antioxidant system and can generate ROS directly through the Fenton reaction or induce ROS accumulation through the mitochondrial pathway. As shown in Table 1, significantly elevated ROS levels exacerbated oxidative stress in muscle tissue ($P < 0.05$), thus validating the intrinsic mechanism by which ferroptosis affects muscle quality through oxidative stress. Heme, another important intracellular Fe^{2+} storage protein, can react with heme oxygenase 1 (HO-1 or HMOX1) to release free Fe^{2+} (Liu et al., 2023). Overall, the down-regulation of ferritin levels (Table 2 and Fig. 3) indicated that it was degraded during refrigeration. The upregulation of HMOX1 (Table 2 and Fig. 3), on the other hand, indicated that heme degradation occurred during refrigeration. Liu et al., (2022) reported that heme degradation during refrigeration released free iron, leading to oxidation of muscle proteins and lipids, further suggesting that heme degradation was caused by HMOX1 degradation. The degradation of iron-containing proteins promoted the release of free iron and iron accumulation, a process also verified by the significant increase of free iron during refrigeration (Table 1). Notably, the valence state of myoglobin, of which heme is a carrier, determines the color of muscle, and myoglobin oxidation drives the conversion of myoglobin to oxymyoglobin and metmyoglobin, and ROS produced during ferroptosis are the promoters of myoglobin oxidation, resulting in the transformation of muscle from a bright red color to a dark red color (Liu et al., 2022; Liu et al., 2023). We thus hypothesize that HMOX1 indirectly accelerates myoglobin oxidation by stretching the spatial structure of myoglobin and promoting the oxidation of the heme porphyrin ring during the degradation of heme.

4.3. PCBP family proteins

Following the release of Fe^{2+} into the cytoplasm via endosomes, Fe^{2+} begins to be regulated by intracellular molecules, as Fe^{2+} can induce cellular oxidative stress via the Fenton reaction (Philpott, Ryu, Frey & Patel, 2017). The intracellular macromolecular ligands, including the Poly rC-binding protein (PCBP) family of iron-binding proteins (mainly PCBP1 and PCBP2), have a strong affinity and can bind Fe^{2+} in a 3:1 ratio to form PCBP-Fe^{2+} complexes. PCBP-Fe^{2+} complexes can bind directly to DMT1. The complex translocates to the cell membrane and

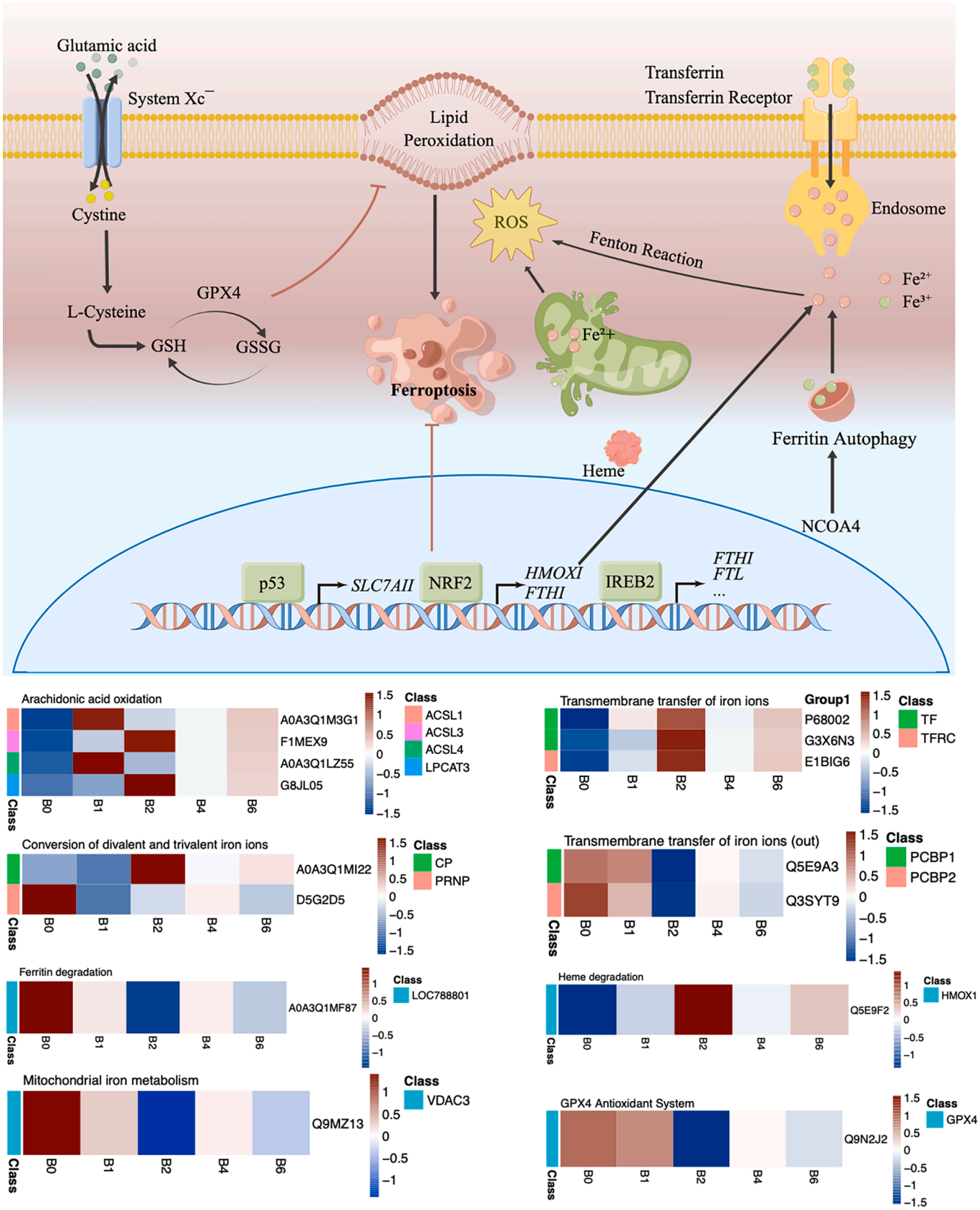

Fig. 3. Mechanism of ferroptosis based on KEGG enrichment of differentially expressed proteins. ACSL1 indicates arachidonate-CoA ligase, ACSL3/4 indicates acyl-CoA synthetase long chain family member 3/4, and LPCAT3 indicates lysophospholipid acyltransferase 5. TF indicates voltage-dependent anion-selective channel protein 2/3 and TFRC indicates transferrin receptor protein 1. CP indicates ceruloplasmin. PRNP indicates major prion protein. PCBP1/2 indicates poly(rC)-binding protein 1/2. LOC788801 indicates ferritin. HMOX1 indicates heme oxygenase 1. VDAC3 indicates voltage-dependent anion-selective channel protein 3. GPX4 indicates phospholipid hydroperoxide glutathione peroxidase.

facilitates the transfer of Fe^{2+} outside the cell. The transport of iron ions from intracellular to extracellular is dependent on the sole membrane iron transport protein (Ferroportin, FPN) and membrane iron transport auxiliary protein (Hephaestin, HP), and PCBP2 binds to Fe^{2+} in the cytoplasm and transfers to the cell membrane to bind to FPN and HP to transfer Fe^{2+} to the extracellular compartment (Yanatori, Richardson, Imada & Kishi, 2016). PCBP2 can also interact with heme oxygenase 1 to bind free iron released from heme. When the intracellular Fe^{2+} concentration increases, PCBP1 binds to the PCBP2-Fe^{2+} complex and is converted into iron storage proteins, such as ferritin, non-heme ferroxidase, 2-oxoglutarate-dependent dioxygenase (with a mononuclear iron center) and fatty acid hydroxylase/desaturase type monooxygenase (with a dinuclear iron center) (Leidgens et al., 2013; Shi, Bencze, Stemmler & Philpott, 2008). A decrease in PCBP2 levels inhibited the FPN-mediated Fe^{2+} translocation process (Table 2 and Fig. 3). In addition, Fe^{2+} transferred to the extracellular compartment is rapidly converted to Fe^{3+} by the action of copper cyanobacteria, and Fe^{3+} bound to transferrin is transferred to the intracellular compartment via the TBI-TFR1 complex, possibly leading to a decrease in intracellular PCBP1/2 levels. Protein expression levels of PCBP1 and PCBP2 were decreased (Table 2 and Fig. 3), indicating a weakening of the binding process to Fe^{2+} macromolecules, which also promotes the accumulation of Fe^{2+} in the cell.

4.4. GSH-GPX4 pathway

GSH is a small molecule that regulates intracellular redox status, and its function of scavenging ROS is critical in the ferroptosis pathway. GSH can bind to Fe2 + via a single thiol ligand of a cysteine residue in the structural domain, limiting its oxidative properties, resulting in significant GSH depletion (Philpott et al., 2017; Qiu, Cao, Cao, Jia & Lu, 2020). Liu et al. (2023) found that the process of ferroptosis in frozen beef was accompanied by a decrease in GSH levels and an increase in oxidized glutathione (GSSH) levels. Reduced intracellular GSH levels make cells more vulnerable to iron overload since they are unable to control ROS produced by the Fenton reaction and other peroxidation processes. GSH can act directly as a tripeptide antioxidant, and more importantly, GSH acts as a cofactor for GPX4 to reduce ROS and inhibit ferroptosis (Wu, Fang, Yang, Lupton & Turner, 2004). GPX4 plays a key role in the regulation of ferroptosis and specifically is the only enzyme that inhibits ferroptosis against oxidation (Forcina et al., 2019). GPX4 protects the cells from damage by catalyzing the reduction reaction of H_2O_2 and hydroperoxides, converting peroxides to water or alcohols. GPX4 is a monomer that can participate in complex lipid peroxidation reactions and also reduces lipid (fatty acid) peroxides, cholesterol peroxides in the hydrogen peroxide phospholipids, and cholesteryl ester peroxides to alcohols for cell protection (Ingold et al., 2018). It was reported that the ferroptosis inducer RSL3 directly bound and inactivated GPX4 to induce ferroptosis, which also validated the important role of GPX4 in the regulation of ferroptosis (Yang et al., 2014). In the study, the down-regulation of GSH levels (Table 1) suggested a decrease of GPX4 function. The down-regulation of GPX4 (Table 2 and Fig. 3) may lead to the enhancement of the ferroptosis process, which was accompanied by a significant increase in ROS levels ($P < 0.05$), and the increase of ROS level suggests a decreased antioxidant capacity of muscle tissue and enhanced muscle tissue oxidation.

4.5. Lipid oxidation pathway

Lipid peroxidation is a hallmark event of ferroptosis, and acyl coenzyme long chain family member (ACSL) 4, lysophosphatidylcholine acyltransferase (LPCAT) 3 and arachidonate-15-lipoxygenase (ALOX15) are known as important enzymes in lipid metabolism that regulate ferroptosis (Zhao et al., 2008). LPCAT3 mediates the reaction between saturated lysophosphatidylcholine and unsaturated fatty acyl-CoAs to induce phosphatidylcholine synthesis, significantly reduces the level of arachidonic acid (AA) in cell membranes and leads to triacylglycerol accumulation and lipid peroxidation, disrupting membrane structure to induce ferroptosis (Forcina & Dixon, 2019). Acyl-CoA synthetase (ACSL) 4 increases the level of long-chain polyunsaturated ω in cell membranes by binding arachidonic acid 6 fatty acids to arachidonic-CoA (AA-CoA) and adrenoic-CoA (AdA-CoA), two long-chain peroxidized polyunsaturated fatty acids (PUFAs)-CoA, leading to impairment of cell membrane or organelle membrane function and induction of cellular ferroptosis (Doll et al., 2017). Both ACSL4 and LPCAT3 protein levels increased during beef storage (Table 2 and Fig. 3), indicating that the activation of AA pathway, and during this process the level of lipid peroxidation product, malondialdehyde increased ($P < 0.05$, Table 1). Lipid is an important component of muscle and one of the most chemically unstable components of the muscular system, and the ferroptosis pathway induces cell death through cell membrane oxidation. Lipid peroxides (MDA, 4-ONE, and 4-HNE, among others) produced by lipid oxidation processes lead to the loss of functional structure of polypeptides, disrupting the structure of proteins and affecting the structural integrity of muscle fiber organization (Mohan, Roy, Duggirala & Klein, 2022).

4.6. Other related pathways

After carcass division, HIF-1α, identified as a differentially expressed gene associated with autophagy and ferroptosis (Hu, Yuan & Wang, 2023), is activated to regulate the ferroptosis process through the HIF-1α-autophagy pathway as the muscle is subjected to hypoxic conditions. Hu et al. (2023) reported that under hypoxic conditions, HIF-1α protein accumulated and translocated to the nucleus to activate its functional target genes. Expression of HIF-1α activates cellular autophagy, which in turn regulates cellular iron homeostasis and cellular ROS production. As iron ions are released at lysosomes, impaired autophagy-lysosomal degradation system may lead to macrophage death and pro-inflammatory factor release and exacerbate the cell death process. Furthermore, Liu et al. (2023) found that treatment of iron-overloaded myocytes using an autophagy inhibitor and inhibition of autophagy resulted in the inhibition of ferroptosis processes. Peroxisome proliferator-activated receptors (PPARs) are essential fatty acid-activated transcription factors. The PPARs network was found to be highly expressed in oxidative tissues and to regulate genes involved in substrate transport and oxidative phosphorylation, as well as in the regulation of energy homeostasis. Among them, PPAR β/δ promotes lipid catabolism in various tissues and acts as a mediator of fatty acid oxidation and fat burning (Christofides, Konstantinidou, Jani & Boussiotis, 2021). It is hypothesized that the PPAR signaling pathway may promote ferroptosis-mediated lipid oxidation processes and induce cell membrane or organelle membrane oxidation. Chemical carcinogenesis - ROS pathway revealed (**Fig. S2**) that ROS induced the heme-HOMX1 ferroptosis pathway by activating Nrf2/HOMX1 expression, and that the free iron released by heme in turn promotes ROS accumulation through the Fenton reaction (Fig. 3).

Overall, ferroptosis is not independent but is regulated by an extremely complex interplay of intracellular metabolic pathways. Some pathways, such as HIF-1, PPARs, cGMP-PKG signaling pathway, calcium signaling pathway, and chemical carcinogenesis-ROS, activate ferroptosis process by regulating oxygen homeostasis, metal ion and ROS accumulation. Porphyrin metabolism and fatty acid degradation further suggest that lipid oxidation and free iron accumulation are the direct causes of ferroptosis. These findings further clarify the mechanism of ferroptosis during refrigeration of beef and provide a new direction for beef quality maintenance and enhancement.

5. Conclusions

TMT quantitative proteomics was used to identify DEPs involved in the regulation of ferroptosis. 15 DEPs were identified as involved in the

ferroptosis pathway. These DEPs were involved in ferric ion transport, Fe^{2+} and Fe^{3+} conversion, lipid oxidation pathway, redox regulation, and iron-containing protein degradation. Overall, ferroptosis pathways were dependent on iron ion accumulation, GPX4 inactivation, and lipid peroxidation. In addition, protein and pathway interaction analysis of the DEPs identified 37 metabolic pathways that promote ferroptosis by regulating cellular iron overload, cell membrane or organelle membrane lipid oxidation, and ROS accumulation. The discovery of ferroptosis mechanism may provide new perspectives for the research related to improving the quality of beef during refrigeration. Also, the identification of the proteins related to ferroptosis may help predict the potential quality of meat and identify biomarkers for ferroptosis.

Funding

This study was financially supported by the Ningxia Natural Science Foundation (2022AAC02021), Hubei Normal University 2023 introduced talent research start-up fund, and Hubei Provincial Natural Science Foundation-Joint Fund Program (2023AFD025).

CRediT authorship contribution statement

Jun Liu: Conceptualization, Data curation, Formal analysis, Investigation, Methodology, Resources, Validation, Visualization, Writing – original draft, Writing – review & editing. **Dunhua Liu:** Funding acquisition, Project administration, Supervision. **Ziying Hu:** Conceptualization, Formal analysis, Visualization, Writing – review & editing. **Yuanliang Hu:** Supervision. **Xiang Yu:** Supervision.

Declaration of Competing Interest

The authors declare that they have no known competing financial interests or personal relationships that could have appeared to influence the work reported in this paper.

Data availability

Data will be made available on request.

Acknowledgments

We thank the Ningxia Provincial Natural Science Foundation (2022AAC02021), Hubei Provincial Natural Science Foundation-Joint Fund Program (2023AFD025), and Hubei Normal University introduced talent research start-up fund for providing financial support for this project. We thank Gaolong Yin at Shanghai Bioprofile Technology Company Ltd. for his technical support in proteomics.

Appendix A. Supplementary data

Supplementary data to this article can be found online at https://doi.org/10.1016/j.foodchem.2023.137596.

References

Christofides, A., Konstantinidou, E., Jani, C., & Boussiotis, V. A. (2021). The role of peroxisome proliferator-activated receptors (PPAR) in immune responses. *Metabolism-Clinical and Experimental, 114*, 154338. https://doi.org/10.1016/j.metabol.2020.154338

Doll, S., Proneth, B., Tyurina, Y. Y., Panzilius, E., Kobayashi, S., Ingold, I., … Conrad, M. (2017). ACSL4 dictates ferroptosis sensitivity by shaping cellular lipid composition. *Nat. Chem. Biol., 13*(1), 91–98. https://doi.org/10.1038/NCHEMBIO.2239

Dowdle, W., Nyfeler, B., Nagel, J., Elling, R., Liu, S., Triantafellow, E., … Murphy, L. (2014). Selective VPS34 inhibitor blocks autophagy and uncovers a role for NCOA4 in ferritin degradation and iron homeostasis in vivo. *Nat. Cell Biol., 16*(11), 1069. https://doi.org/10.1038/ncb3053

Forcina, G., & Dixon, S. (2019). GPX4 at the Crossroads of Lipid Homeostasis and Ferroptosis. *Proteomics, 19*(18), 1800311. https://doi.org/10.1002/pmic.201800311

Gagaoua, M., Terlouw, E. M. C., & Picard, B. (2017). The study of protein biomarkers to understand the biochemical processes underlying beef color development in young bulls. *Meat Sci., 134*, 18–27.

Gaschler, M. M., & Stockwell, B. R. (2017). Lipid peroxidation in cell death. *Biochem. Biophys. Res. Commun., 482*(3), 419–425. https://doi.org/10.1016/j.bbrc.2016.10.086

Guo, B., Zhang, W., Tume, R. K., Hudson, N. J., Huang, F., Yin, Y., & Zhou, G. (2016). Disorder of endoplasmic reticulum calcium channel components is associated with the increased apoptotic potential in pale, soft, exudative pork. *Meat Sci., 115*, 34–40. https://doi.org/10.1016/j.meatsci.2016.01.003

Hu, G., Yuan, Z., & Wang, J. (2023). Autophagy inhibition and ferroptosis activation during atherosclerosis: Hypoxia-inducible factor 1α inhibitor PX-478 alleviates atherosclerosis by inducing autophagy and suppressing ferroptosis in macrophages. *Biomed. Pharmacother., 161*, 114333. https://doi.org/10.1016/j.biopha.2023.114333

Ingold, I., Berndt, C., Schmitt, S., Doll, S., Poschmann, G., Buday, K., … Conrad, M. (2018). Selenium utilization by GPX4 is required to prevent hydroperoxide-induced ferroptosis. *Cell, 172*, 409. https://doi.org/10.1016/j.cell.2017.11.048

Jia, W., Shi, Q., Zhang, R., Shi, L., & Chu, X. (2021). Unraveling proteome changes of irradiated goat meat and its relationship to off-flavor analyzed by high-throughput proteomics analysis. *Food Chem., 337*. https://doi.org/10.1016/j.foodchem.2020.127806

Jia, W., Zhang, R., Liu, L., Zhu, Z., Xu, M., & Shi, L. (2021). Molecular mechanism of protein dynamic change for Hengshan goat meat during freezing storage based on high-throughput proteomics. *Food Res. Int., 143*. https://doi.org/10.1016/j.foodres.2021.110289

Joseph, P., Nair, M. N., & Suman, S. P. (2015). Application of proteomics to characterize and improve color and oxidative stability of muscle foods. *Food Res. Int., 76*, 938–945. https://doi.org/10.1016/j.foodres.2015.05.041

Lana, A., Longo, V., Dalmasso, A. D., Alessandro, A., Bottero, M. T., & Zolla, L. (2015). Omics integrating physical techniques: Aged Piedmontese meat analysis. *Food Chem., 172*, 731–741. https://doi.org/10.1016/j.foodchem.2014.09.146

Leidgens, S., Bullough, K., Shi, H., Li, F., Shakoury-Elizeh, M., Yabe, T., … Philpott, C. (2013). Each member of the poly-r(C)-binding protein 1 (PCBP) family exhibits iron chaperone activity toward ferritin. *J. Biol. Chem., 288*(24), 17791–17802. https://doi.org/10.1074/jbc.M113.460253

Liu, J., Ellies-Oury, M., Stoyanchev, T., & Hocquette, J. (2022). Consumer perception of beef quality and how to control, improve and predict it? *Focus on Eating Quality. Foods, 11*(12), 1732. https://doi.org/10.3390/foods11121732

Liu, J., Hu, Z., Liu, D., Zheng, A., & Ma, Q. (2023). Glutathione metabolism-mediated ferroptosis reduces water-holding capacity in beef during cold storage. *Food Chem., 398*, 133903. https://doi.org/10.1016/j.foodchem.2022.133903

Liu, J., Hu, Z., Ma, Q., Wang, S., & Liu, D. (2023). Ferritin-dependent cellular autophagy pathway promotes ferroptosis in beef during cold storage. *Food Chem., 412*, 135550. https://doi.org/10.1016/j.foodchem.2023.135550

Liu, J., Hu, Z., Ma, Q., Yang, C., Zheng, A., & Liu, D. (2023). Reduced water-holding capacity of beef during refrigeration is associated within creased heme oxygenase 1 expression, oxidative stress and ferroptosis. *Meat Sci., 202*, 109202. https://doi.org/10.1016/j.meatsci.2023.109202

Liu, J., Liu, D., Wu, X., Pan, C., Wang, S., & Ma, L. (2022). TMT quantitative proteomics analysis reveals the effects of transport stress on iron metabolism in the liver of chicken. *Animals, 12*(1), 52. https://doi.org/10.3390/ani12010052

Liu, J., Liu, D., Zheng, A., & Ma, Q. (2022). Haem-mediated protein oxidation affects water-holding capacity of beef during refrigerated storage. *Food Chemistry: X, 100304*. https://doi.org/10.1016/j.fochx.2022.100304

Luan, Y., Dong, Y., Duan, X., Wang, X., Pang, Y., Li, Q., & Gou, M. (2022). TMT-based quantitative proteomics reveals protein biomarkers from cultured Pacific abalone (Haliotis discus hannai) in different regions. *Food Chemistry: X, 14*, 100355. https://doi.org/10.1016/j.fochx.2022.100355

Ma, T., Chen, J., Zhu, P., Zhang, C., Zhou, Y., & Duan, J. (2022). Focus on ferroptosis regulation: Exploring novel mechanisms and applications of ferroptosis regulator. *Life Sci., 120868*. https://doi.org/10.1016/j.lfs.2022.120868

Mancias, J. D., Wang, X., Gygi, S. P., Harper, J. W., & Kimmelman, A. C. (2014). Quantitative proteomics identifies NCOA4 as the cargo receptor mediating ferritinophagy. *Nature, 509*(7498), 105–109. https://doi.org/10.1038/nature13148

Mohan, A., Roy, A., Duggirala, K., & Klein, L. (2022). Oxidative reactions of 4-oxo-2-nonenal in meat and meat products. *LWT, 165*, 113747. https://doi.org/10.1016/j.lwt.2022.113747

Philpott, C. C., Ryu, M., Frey, A., & Patel, S. (2017). Cytosolic iron chaperones: Proteins delivering iron cofactors in the cytosol of mammalian cells. *J. Biol. Chem., 292*(31), 12764–12771. https://doi.org/10.1074/jbc.R117.791962

Pogorzelski, G., Pogorzelska-Nowicka, E., Pogorzelski, P., Półtorak, A., Hocquette, J., & Wierzbicka, A. (2022). Towards an integration of pre- and post-slaughter factors affecting the eating quality of beef. *Livest. Sci., 255*, 104795. https://doi.org/10.1016/j.livsci.2021.104795

Qiu, Y., Cao, Y., Cao, W., Jia, Y., & Lu, N. (2020). The application of ferroptosis in diseases. *Pharmacol. Res., 159*. https://doi.org/10.1016/j.phrs.2020.104919

Shi, H., Bencze, K., Stemmler, T., & Philpott, C. (2008). A cytosolic iron chaperone that delivers iron to ferritin. *Science, 320*(5880), 1207–1210. https://doi.org/10.1126/science.1157643

Stoyanovsky, D. A., Tyurina, Y. Y., Shrivastava, I., Bahar, I., Tyurin, V. A., Protchenko, O., … Kagan, V. E. (2019). Iron catalysis of lipid peroxidation in ferroptosis: Regulated enzymatic or random free radical reaction? *Free Radic. Biol. Med., 133*, 153–161. https://doi.org/10.1016/j.freeradbiomed.2018.09.008

Tian, Z., Li, X., Shi, X., & Chen, C. (2022). Effects of nitric oxide synthase inhibitor on mitochondria apoptosis and meat quality in postmortem Gannan yak (Bos grunniens) meat. *J. Food Biochem., 46*(9), e14234. https://doi.org/10.1111/jfbc.14234

Wu, G., Fang, Y., Yang, S., Lupton, J., & Turner, N. (2004). Glutathione metabolism and its implications for health. *J. Nutr., 134*(3), 489–492. https://doi.org/10.1093/jn/134.3.489

Xiong, L., Zhou, B., Young, J. L., Wintergerst, K., & Cai, L. (2022). Exposure to low-dose cadmium induces testicular ferroptosis. *Ecotoxicol. Environ. Saf., 234*, 113373. https://doi.org/10.1016/j.ecoenv.2022.113373

Yanatori, I., Richardson, D. R., Imada, K., & Kishi, F. (2016). Iron export through the transporter ferroportin 1 Is modulated by the iron chaperone PCBP2*. *J. Biol. Chem., 291*(33), 17303–17318. https://doi.org/10.1074/jbc.M116.721936

Yang, W. S., SriRamaratnam, R., Welsch, M. E., Shimada, K., Skouta, R., Viswanathan, V. S., … Stockwell, B. R. (2014). Regulation of ferroptotic cancer cell death by GPX4. *Cell, 156*(1–2), 317–331. https://doi.org/10.1016/j.cell.2013.12.010

Yang, W. S., & Stockwell, B. R. (2016). Ferroptosis: Death by lipid peroxidation. *Trends Cell Biol., 26*, 165. https://doi.org/10.1016/j.tcb.2015.10.014

Zhang, J., Yu, Q., Han, L., Han, M., & Han, G. (2020). Effects of lysosomal iron involvement in the mechanism of mitochondrial apoptosis on postmortem muscle protein degradation. *Food Chem., 328*, 127174. https://doi.org/10.1016/j.foodchem.2020.127174

Zhang, M., Wang, D., Huang, W., Liu, F., Zhu, Y., Xu, W., & Cao, J. (2013). Apoptosis during postmortem conditioning and its relationship to duck meat quality. *Food Chem., 138*(1), 96–100. https://doi.org/10.1016/j.foodchem.2012.10.142

Zhao, N., Gao, J., Enns, C. A., & Knutson, M. D. (2010). ZRT/IRT-like protein 14 (zip14) promotes the cellular assimilation of iron from transferrin. *J. Biol. Chem., 285*(42), 32141–32150. https://doi.org/10.1074/jbc.M110.143248

Zhao, Y., Chen, Y., Bonacci, T., Bredt, D., Li, S., Bensch, W., … Cao, G. (2008). Identification and characterization of a major liver lysophosphatidylcholine acyltransferase. *J. Biol. Chem., 283*(13), 8258–8265. https://doi.org/10.1074/jbc.M710422200